Journal of Power Sources 196 (2011) 7343–7346

Contents lists available at ScienceDirect

Journal of Power Sources

journal homepage: www.elsevier.com/locate/jpowsour

Short communication

Performance simulation of current/voltage-characteristics for SOFC single cell by means of detailed impedance analysis

A. Leonide[a,*], S. Hansmann[a], André Weber[a], E. Ivers-Tiffée[a,b]

[a] Institut für Werkstoffe der Elektrotechnik (IWE), Karlsruhe Institute of Technology (KIT), D-76131 Karlsruhe, Germany
[b] DFG Center for Functional Nanostructures (CFN), Karlsruhe Institute of Technology (KIT), D-76131 Karlsruhe, Germany

ARTICLE INFO

Article history:
Received 30 June 2010
Received in revised form 13 October 2010
Accepted 18 October 2010
Available online 23 October 2010

Keywords:
Solid oxide fuel cell
Anode-supported
Impedance
Stationary
Modeling
Performance

ABSTRACT

We present a zero dimensional stationary model which precisely predicts the current–voltage-characteristics of anode supported SOFC single cells over a wide range of operating conditions. The different kinds of electrode polarization resistances are separated from experimental impedance data by means of a detailed equivalent circuit model developed specifically for the analyzed cell type. The activation losses are modeled by the Butler–Volmer equation, whereas the loss contributions from gas diffusion polarizations are calculated from Fick's law. The partial pressure and temperature dependency of the cathodic and anodic exchange current density could be determined by a fit of semi empirical power law model equations. The exponents *c* and *d* for the CO and CO_2 partial pressure dependency of the anodic exchange current density are determined independently of each other. This paper presents the modeling results for a wide range of operation parameters as well as their experimental verification.

1. Introduction

Interest in solid oxide fuel cells (SOFC), which combine potentially efficient energy production with flexible fuel composition, has significantly increased in the past few years. Amongst the most important development goals is, besides long-term stability, the single-cell performance, which is limited by three loss mechanisms: (i) ohmic losses, (ii) polarization losses through gas diffusion, and (iii) losses by activation polarization.

In this study the different loss mechanisms and their contributions are identified and subsequently separated by means of impedance spectroscopy in combination with a fit of the measured spectra to a detailed equivalent circuit model developed specifically for the cell type investigated and presented in Ref. [1]. The parameters determined in this manner are used to predict the current–voltage (*I–U*) characteristics of the analyzed anode supported SOFC single cells (ASCs) in a broad range of operating conditions [2] (Fig. 1).

2. Experimental

The ASCs investigated are based on 50 mm × 50 mm anode substrates (Ni/8YSZ, thickness 1 mm), an anode functional layer (Ni/8YSZ, thickness approximately 7 μm), a thin film electrolyte (8YSZ, thickness approximately 10 μm) and a $Ce_{0.8}Gd_{0.2}O_{2-\delta}$ (CGO) interlayer (thickness approximately 10 μm). The $La_{0.58}Sr_{0.4}Co_{0.2}Fe_{0.8}O_{3-\delta}$ cathodes (1 cm × 1 cm, thickness approximately 45 μm) were deposited by screen printing and subsequently sintered. Detailed information on preparation and properties of these cells is given in Refs. [2–5].

The cells were characterized by electrochemical impedance spectroscopy (EIS) in a wide range of operating conditions (various temperatures and partial pressures of carbon monoxide and carbon dioxide (pCO, pCO_2)). The EIS measurements were carried out with a Solartron 1260 FRA in the frequency range from 30 mHz to 1 MHz.

I–U measurements were carried out at temperatures between 650 °C and 800 °C with current densities up to 2 A cm^{-2} and cell voltages not below a limit of 0.6 V. This operation range guaranties a stable cell performance during all experiments.

The single cells were investigated under ambient air pressure at various gas compositions of CO, CO_2, and N_2 at the anode side. Pure air was used on the cathode side. The overall gas flow rate was constantly kept at 250 ml min^{-1} for the anode as well as the cathode. These fairly high flow rates were chosen to assure constant gas compositions, i.e. a "low" fuel utilization within the entire cell area. For cell voltages not lower than 0.6 V a maximum fuel utilization of about 9% can be calculated. For the analyzed operating conditions the latter corresponds to a maximum voltage drop due to fuel utilization not higher than 10 mV (calculated by the Nernst

* Corresponding author. Tel.: +49 7216086484; fax: +49 7216087492.
E-mail address: andre.leonide@kit.edu (A. Leonide).

0378-7753/$ – see front matter © 2010 Elsevier B.V. All rights reserved.
doi:10.1016/j.jpowsour.2010.10.052

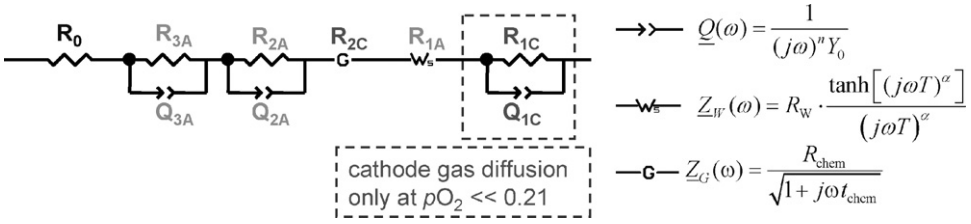

Fig. 1. Equivalent circuit model used for the CNLS fit of impedance data [1].

equation). For this reason in the present work the voltage drop due to gas conversion has been neglected.

3. Evaluation of impedance spectra

The measured impedance curves were evaluated using the commercially available complex nonlinear least squares (CNLS) fit software Z-View [6]. The equivalent-circuit model used for this procedure (Fig. 1) was developed by a pre-identification of the impedance response by calculating and analyzing the corresponding distribution of relaxation times (DRT) and has been presented in Refs. [1,2,7–9]. For a more detailed description of the DRT method and its application we refer the reader to Ref. [10].

The applied equivalent circuit (Fig. 1) consists of 5 serial impedance elements: (i) an ohmic resistor (R_0: ohmic losses), (ii) two serial RQ elements (R_{2A} and R_{3A}: gas diffusion and activation polarization in the anode functional layer [1,7,9,11]), (iii) a Gerischer element [12] (R_{2C}: activation polarization of the cathode), (iv) a generalized finite length Warburg Element (G-FWS) (R_{1A}: gas diffusion polarization in the anode substrate), and (v) an RQ element (R_{1C}: diffusion polarization in the cathode), which, however, significantly contributes to the equivalent circuit only at very low cathode oxygen partial pressures ($pO_{2,cat} < 0.05$ atm), cf. Table 1.

At this point it is needed to specify, that the gas diffusion loss inside the 7 μm thick anode functional layer (AFL) can be neglected after appositely activating the cell: The AFL is a dense layer after initial reduction. It lasts several hours (approx. 150 h) of cell operation until a certain open porosity in the AFL structure is reached. From there on gas diffusion in the AFL can be neglected for cells with an AFL thickness smaller than 8 μm, i.e. for the cell type analyzed within this study [7,9].

With the help of this equivalent-circuit model, the measured impedance spectra could be separated into the single loss contributions, thus permitting a precise determination of the area-specific resistance values for the single loss contributions of the analyzed ASCs (Table 1). This procedure is the basis for the experimental determination of the modeling parameters.

4. Results and discussion

In this paper the *I–U* characteristics are modeled using the Butler–Volmer equation, Fick's law as well as Ohm's law. The partial pressure dependency of the exchange current densities $j_{0,an}$ and $j_{0,cat}$ of anode and cathode, respectively, are described by a semi-empirical power law ansatz. The temperature dependency of the ohmic resistance and of the exchange current densities ($j_{0,an}$ and $j_{0,cat}$) is modeled by an Arrhenius ansatz. The complete set of equations is shown in Table 2. For more details on the model the reader is referred to Ref. [2].

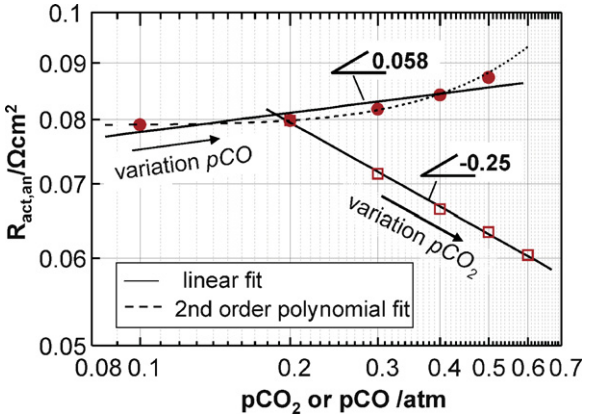

Fig. 2. Determination of parameters c and d. $R_{act,an} = R_{2A} + R_{3A}$ as a function of pCO (at fixed $pCO_2 = 0.20$ atm, balance N_2) and pCO_2 (at fixed pCO = 0.40 atm, balance N_2) on a double-logarithmic scale ($T = 800\,^{\circ}C$).

In order to make a prediction of the anodic activation polarization overvoltage ($\eta_{act,an}$) the prefactor γ_{an}, the exponents c and d, as well as the activation energy $E_{act,an}$ have to be determined (cf. equations in Table 2). The exponents c and d for the pCO and pCO_2 dependency are determined separately in this study. To ensure that pCO and pCO_2 could be varied independently of each other, a defined amount of inert gas (N_2) was added to the gas mixture.

In Fig. 2 the resistances $R_{act,an}(pCO_{an})$ and $R_{act,an}(pCO_{2,an})$ are plotted, respectively, as a function of partial pressure on a double-logarithmic scale. The parameters $c = -0.058$ and $d = 0.25$ can be extracted from the negative value of the slope of the linear fit, in each case. The negative sign is a result of the inverse proportionality between exchange current density and the resistance (see Table 2).

To determine the unknown parameters γ_{an}, $E_{act,an}$, B_{ohm} and $E_{act,ohm}$, impedance measurements were carried out at different temperatures (650–800 °C). The ohmic and activation polarization resistances $R_{ohm} \equiv R_0$ and $R_{act,an} \equiv R_{2A} + R_{3A}$ resulting from the CNLS fit are shown in Fig. 3 as a function of temperature. These resistances were, in turn, fitted with the Arrhenius equation (cf. Table 2). In this way the parameters $\gamma_{an} = (4.56 \times 10^6 T)\,A\,m^{-2}$, $E_{act,an} = 118.64\,kJ\,mol^{-1}$ (1.23 eV),

Table 1
List of the processes known to take place in a ASC, together with their temperature and frequency dependencies as well as the characteristic frequency (f_r) range [2].

Process	f_r	Dependencies	Physical origin
P_{1C}	0.3–10 Hz	pO_2, temperature (low)	Gas diffusion in the cathode structure and gas flow channel
P_{2C}	7–500 Hz	pO_2, temperature	Oxygen surface exchange kinetics and O^{2-}-diffusivity in the bulk of the cathode
P_{1A}	0.070–10 Hz	pH_2, pH_2O, pCO, pCO_2, temperature (low)	Gas diffusion in the anode substrate
P_{2A} P_{3A}	200 Hz–3 kHz3–50 kHz	pH_2, pH_2O, pCO, pCO_2, temperature	($P_{2A} + P_{3A}$) gas diffusion coupled with charge transfer reaction and ionic transport (AFL: anode functional layer) [1,7,9,11]

Table 2
List of model equations from [2].

Open circuit voltage (OCV)	$U_{OCV}(T) = U_0(T) - \frac{RT}{2F} \ln\left(\frac{pCO_{2,an}}{pCO_{an}\cdot\sqrt{pO_{2,cat}}}\right)$
Cell voltage (U_{cell})	$U_{cell} = U_{OCV} - (\eta_{ohm} + \eta_{act,an} + \eta_{act,cat} + \eta_{conc,an} + \eta_{conc,cat})$
Anode and cathode gas diffusion overpotential ($\eta_{conc,el}$) [13,14]	$\eta_{conc,cat} = \frac{RT}{4F} \ln\left(\frac{1}{1-(RTL_{cat}(1-pO_{2,cat}))/4FD^{eff}_{O_2} P_0 pO_{2,cat})\cdot j}\right)$
	$\eta_{conc,an} = \frac{RT}{2F} \ln\left(\frac{1+(RTL_{an}/2FD^{eff}_{CO_2} P_0 pCO_{2,an})\cdot j}{1-(RTL_{an}/2FD^{eff}_{CO} P_0 pCO_{an})\cdot j}\right)$; $P_0 = 1.0133\times10^5$ Pa/atm
	with $D_i^{eff} = \psi_{an/cat}\cdot D_{mol,i}$
Butler–Volmer [15–19] and power law equations [20] for calculating the activation overpotential ($\eta_{act,el}$)	$j = j_{0,el}\left[\exp\left(\alpha_{el}\frac{neF\eta_{act,el}}{RT}\right) - \exp\left(-(1-\alpha_{el})\frac{neF\eta_{act,el}}{RT}\right)\right]$ with $j_{0,cat} = \gamma_{cat}(pO_{2,cat})^m \exp\left(-\frac{E_{act,cat}}{RT}\right)$
	and $j_{0,an} = \gamma_{an}(pCO_{an})^c(pCO_{2,an})^d \exp\left(-\frac{E_{act,an}}{RT}\right)$
Relation between $j_{0,el}$ and $R_{act,el}$	$\frac{d\eta_{act,el}}{dj}\Big\vert_{j=0} = \frac{RT}{2F\cdot j_{0,el}} = R_{act,el}$ with $R_{act,an} \equiv R_{2A} + R_{3A}$ and $R_{act,cat} \equiv R_{2C}$
Ohmic overpotential (η_{ohm}) [21,22]	$\eta_{ohm} = j\cdot R_{ohm}$ with $R_{ohm}(T) = \frac{T}{B_{ohm}}\exp\left(\frac{E_{act,ohm}}{RT}\right)$ with $R_{ohm} \equiv R_0$

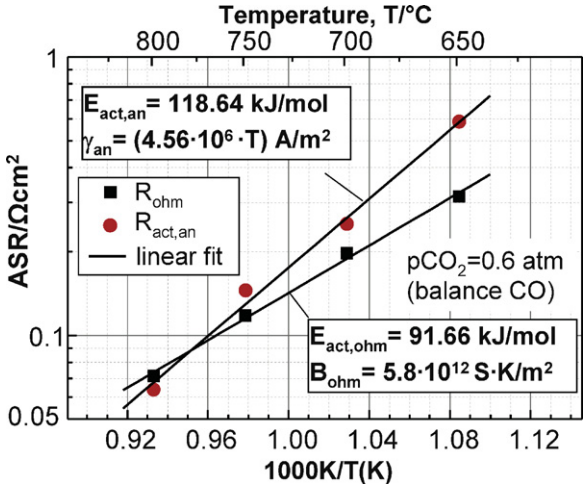

Fig. 3. Determination of parameters γ_{an}, $E_{act,an}$, B_{ohm} and $E_{act,ohm}$. Arrhenius plots of $R_{act,an} = R_{2A} + R_{3A}$ and $R_{ohm} = R_0$.

$B_{ohm} = 5.8\times10^{12}$ S K m^{-2} and $E_{act,ohm} = 91.66$ kJ mol^{-1} (0.95 eV) are obtained (cf. Fig. 3 and Table 3).

The structural parameters $\psi_{an} = 0.133$ and $\psi_{cat} = 0.022$ for the calculation of the gas diffusion polarization and the parameters $\gamma_{cat} = (1.52\times10^8 T)$ A m^{-2}, $m = 0.22$, $\alpha_{cat} = 0.65$ and $E_{act,cat} = 139.86$ kJ mol^{-1} for the calculation of the cathodic exchange current density $j_{0,cat}$ were already determined in a previous study (on nominally identical cells), and thus adopted here [2]. Therefore, the sole remaining parameter to be determined is the charge transfer coefficient α_{an}. Different to the previous procedure, this parameter is obtained by impedance measurements under load, since the charge transfer coefficient affects the current-dependent behavior of the activation overpotential. α_{an} was obtained by a (polynomial) fit of the evaluated current dependent $R_{act,an}$ followed by a least-squares-fit of the Butler–Volmer equation (for details on this procedure the reader is referred to Ref. [2]). The value determined in this way ($\alpha_{an} = 0.62$) is listed in Table 3.

To validate the model, *I–U* characteristics were recorded at different temperatures and gas compositions. In Fig. 4a and b the measured and predicted *I–U* curves are compared. As can be seen, the model delivers a very reliable prediction of the measured curves over the entire parameter range.

At high operating temperatures the electrochemical reactions at the electrodes are faster, as a result the overpotentials due

Table 3
Modeling parameters determined from impedance measurements.

Parameter	Value/expression	Unit	Comment
B_{ohm}	5.8×10^{12}	S K m^{-2}	
$E_{act,ohm}$	91.66	kJ mol^{-1}	
c	−0.058	–	
d	0.25	–	
m	0.22	–	Adopted from [2]
γ_{an}	$4.56\times10^6\times T$	A m^{-2}	
γ_{cat}	$1.52\times10^8\times T$	A m^{-2}	Adopted from [2]
$E_{act,an}$	118.64	kJ mol^{-1}	
$E_{act,cat}$	139.86	kJ mol^{-1}	Adopted from [2]
α_{an}	0.62	–	
α_{cat}	0.65	–	Adopted from [2]
ψ_{an}	0.133	–	Adopted from [2]
ψ_{cat}	0.022	–	Adopted from [2]

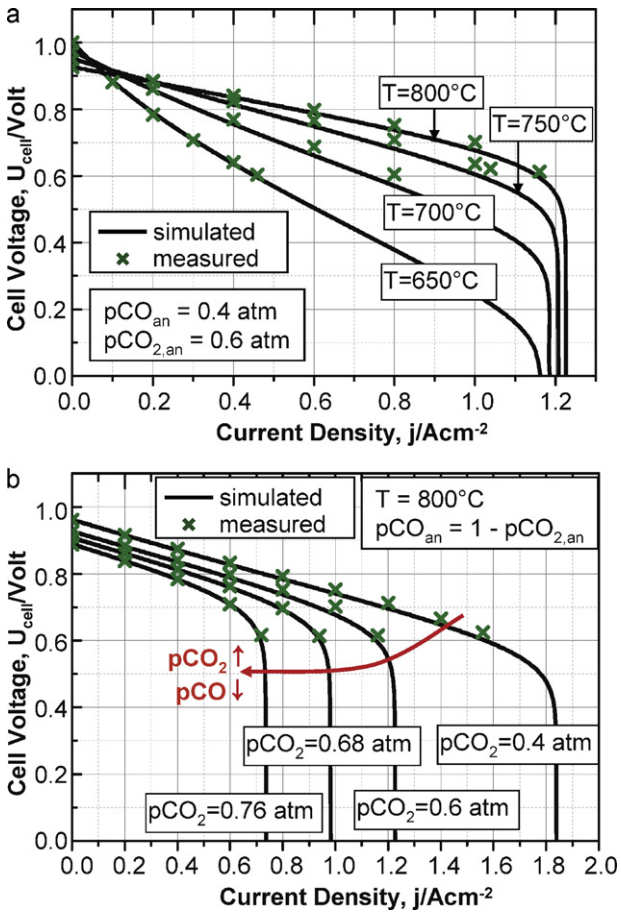

Fig. 4. Simulated (lines) and measured (symbols) *I–U* curves at four different temperatures (a) and gas compositions (b).

to activation polarization are lower. Moreover, the temperature dependence of the ohmic losses $R_{ohm}(T)$ exhibit an Arrhenius-type behavior, which also leads to lower ohmic losses at high temperatures. However, higher temperatures also yield lower open-circuit voltages. These temperature-dependent characteristics typical of the *I–U* curves can be observed for all predicted curves (Fig. 4a).

By analyzing Fig. 4a it can be seen that the model traces beyond the cell voltage of 0.6 V are approaching a limiting current density (at $U_{cell} = 0$) which is weakly dependent on temperature. This behavior can be explained by the fact that the gas diffusion polarization is characterized by a negligible dependency on temperature as already discussed in Refs. [1,2,13].

Fig. 4b shows the simulation results for different CO and CO_2 partial pressures at a constant temperature ($T = 800\,^{\circ}C$) and oxygen partial pressure at the cathode ($pO_{2,cat} = 0.21$ atm (air)). Low CO partial pressures were approached appositely to validate the model within the diffusion limitation regime of the *I–U* characteristics. For the cell type investigated, gas diffusion polarization at the anode becomes already predominant at carbon monoxide partial pressures $pCO_{an} < 0.4$ atm. A comparison between simulated and measured *I–U* curves at $pCO_{an} = 0.24$ atm clearly shows that the diffusion overpotential at the anode predicted by the model is sufficiently precise.

5. Conclusions

A zero-dimensional stationary model for the prediction of current–voltage characteristics of planar anode-supported SOFC single cells operated on CO has been presented. Simulation results show a very good agreement with experimentally determined data. The model is based on the Butler–Volmer equation for the determination of activation polarization, Fick's model, using the calculation of the structural parameters (ψ_{an} and ψ_{cat}), for obtaining the diffusion polarization, and, lastly, Ohm's law for calculating the ohmic overpotential. The necessary modeling parameters were all obtained from impedance measurements, thereby specifically varying the operating conditions, e.g. fuel composition at the anode, oxidizing gas composition at the cathode, current load density and temperature.

However, the model only yields precise results assuming a spatially constant current density and temperature distribution throughout the active electrode area which requires cells with a sufficiently small cross-sectional area (1 cm^2 electrodes in our case). Moreover, in the future the model shall be employed for the prediction of the performance of larger single cells (stack-"repeating units"). For this purpose, it has to be expanded into a two-dimensional model in order to consider a spatially resolved current density and the resulting in-plane temperature distribution of the cell. Of course, in case of larger cells the voltage drop due to the fuel utilization, which has been neglected so far, has to be considered.

References

[1] A. Leonide, V. Sonn, A. Weber, E. Ivers-Tiffée, J. Electrochem. Soc. 155 (2008) B36.
[2] A. Leonide, Y. Apel, E. Ivers-Tiffée, ECS Trans. 19 (2009) 81–109.
[3] D. Stöver, H.P. Buchkremer, J.P.P. Huijsmans, in: W. Vielstich, A. Lamm, H.A. Gasteiger (Eds.), Handbook of Fuel Cells, Volume 4: Fuel Cell Technology and Applications Part 2, John Wiley and Sons Ltd., Chichester, UK, 2003, pp. 1013–1031.
[4] H.P. Buchkremer, U. Diekmann, D. Stöver, in: B. Thorstensen (Ed.), Proc. 2nd European Solid Oxide Fuel Cell Forum, European Fuel Cell Forum, vol. 221, Oberrohrdorf, Switzerland, 1996.
[5] M. Becker, A. Mai, E. Ivers-Tiffée, F. Tietz, in: S.C. Singhal J. Mizusaki (Eds.), Solid Oxide Fuel Cells IX, PV 2005–07, The Electrochemical Society Proceeding Series, Pennington, NJ (2005) 514.
[6] D. Johnson, ZPlot, ZView Electrochemical Impedance Software, Version 2.3b, Scribner Associates Inc., 2000.
[7] C. Endler, A. Leonide, A. Weber, F. Tietz, E. Ivers-Tiffée, J. Electrochem. Soc. 157 (2010) B292.
[8] A. Leonide, B. Rüger, W.A. Meulenberg, A. Weber, F. Tietz, E. Ivers-Tiffée, J. Electrochem. Soc. 157 (2010) B234.
[9] A. Leonide, S. Ngo Dinh, A. Weber, E. Ivers-Tiffée, in: R. Steinberger-Wilckens, U. Bossel (Eds.), 8th European Solid Oxide Fuel Cell Forum, Oberrohrdorf, Switzerland, 2008, A0501.
[10] H. Schichlein, A.C. Müller, M. Voigts, A. Krügel, E. Ivers-Tiffée, J. Appl. Electrochem. 32 (2002) 875.
[11] V. Sonn, A. Leonide, E. Ivers-Tiffée, J. Electrochem. Soc. 155 (2008) B675.
[12] S.B. Adler, J.A. Lane, B.C.H. Steele, J. Electrochem. Soc. 143 (1996) 3554.
[13] S. Primdahl, M. Mogensen, J. Electrochem. Soc. 146 (1999) 2827.
[14] J.W. Kim, A.V. Virkar, K.Z. Fung, K. Mehta, S.C. Singhal, J. Electrochem. Soc. 146 (1999) 69.
[15] A.V. Virkar, J. Chen, C.W. Tanner, J.W. Kim, Solid State Ionics 131 (2000) 189.
[16] P. Aguiar, C.S. Adjiman, N.P. Brandon, J. Power Sources 138 (2004) 120.
[17] A.V. Akkaya, Int. J. Energy Res. 31 (2007) 79.
[18] Y. Wang, F. Yoshiba, T. Watanabe, S.L. Weng, J. Power Sources 170 (2007) 101.
[19] A.J. Bard, L.R. Faulkner, Electrochemical Methods, John Wiley & Sons, New York, 2001.
[20] H. Wendt, G. Kreysa, Electrochemical Engineering, Springer, Berlin, 1999.
[21] A.C. Müller, J.R. Opfermann, E. Ivers-Tiffée, Thermochim. Acta 414 (2004) 11.
[22] D. Sanchez, R. Chacartegui, A. Munoz, T. Sanchez, J. Power Sources 160 (2006) 1074.